Composites Part A: Applied Science and Manufacturing
October 2022, Volume 161 Pages 107105 (10p.)
https://doi.org/10.1016/j.compositesa.2022.107105
https://archimer.ifremer.fr/doc/00787/89850/

Effect of aging on the fatigue crack growth properties of carbon-polyamide 6 thermoplastic composites using the multi ΔG-control method

Arhant Mael [1, *], Lolive Eric [2], Bonnemains Thomas [2], Davies Peter [1]

[1] IFREMER Centre de Bretagne, Marine Structures Laboratory, Centre de Bretagne, Plouzané, France
[2] IUT de Brest, IRDL, Brest, France

* Corresponding author : Mael Arhant, email address : mael.arhant@ifremer.fr

Abstract :

This paper focuses on the fatigue crack growth behavior of unidirectional C/PA6 composites subjected to hydrolytic aging at temperatures ranging from 100 to 140 °C. The fatigue crack growth properties were determined using a multi-ΔG control test method. The latter is fully automatic and allows measurement of crack growth rates at various ΔG levels. It was shown that the fatigue crack growth properties were highly affected by aging. Whatever the aging temperature, the crack growth rate was increased by about a decade after aging, and the fatigue crack growth properties are highly dependent on the molar mass. Finally, it was shown that the traditional Paris law does not allow a full description of the behaviour so the Hartman-Schijve relationship was applied to characterize the fatigue response.

Highlights

► The multi-ΔG control method was successfully used to investigate the effect of hydrolytic aging on fatigue crack growth properties. ► The Hartman-Schijve relationship accurately describes the changes in mechanical behaviour induced by wet aging. ► Fatigue crack growth properties are highly dependent on the molar mass M_n. ► Fatigue crack growth properties are more sensitive to aging than quasi-static fracture toughness.

Keywords : Thermoplastic composites, Fatigue crack growth, Hydrolysis, Molar mass

1. Introduction

Composite materials are now used in many industrial applications (aviation, military, renewable energy, nuclear, marine, etc.). Over the past 40 years, the fatigue behavior of these materials has become a major subject due to unexpected failures. Indeed, in many cases, the design of composite structures is carried out using experimental data from static tests, which can be insufficient; these values are affected by both the service environment and the loading conditions. Design for long term applications should therefore be based on more appropriate values. It is therefore necessary to consider fatigue loadings in design and to do so, accurate experimental fatigue data are essential. One specific damage mechanism of composite materials is delamination, due to their layered structure, and this can be critical under cyclic loads.

The fatigue crack growth properties of composite materials have received considerable attention in the published literature [1, 2], and several tests methods to determine these properties were proposed [3-6]. A fatigue crack growth test can be performed under various different conditions, for example: controlled using constant displacement (mostly used), load, or energy. The latter has received some interest in the 1990s [7,8]. However, it is only recently that the subject has been revisited, with the work of Sato [9] and then Manca [10]. Manca's method is based on compliance monitoring, which implies the continuous adjustment of the maximum and minimum displacements throughout the test. This allows a constant energy ΔG to be applied. Recently, the authors [11] extended this method to a multi-ΔG control test, so that it is possible to obtain the crack growth rate for various constant ΔG values with only one specimen. A major advantage of this method is that once the algorithm is implemented in a given software, it is completely automated. Additionally, it was shown that the experimental data can be described using the Hartman-Schijve relationship [12], i.e. an evolved equation of the Paris law [13]. The latter was initially used to describe the fatigue crack growth in metals and was recently extended to adhesives [14] and composites [15].

Another aspect known to limit the life of composite structures is the aging of these materials when subjected to a harsh environment (high temperatures and sea water for example). In the literature, a significant amount of work is found on the subject [16, 17], more especially concerning thermoset based composites and their fatigue crack growth properties.

For neat polymers, it is well known that during aging the molar mass can decrease, due to chain scission (from oxidation or hydrolysis). It was also demonstrated that the static mechanical properties can be directly linked with the molar mass in PTFE [18], polyethylene [19], polypropylene [20], polyethylene terephthalate [21] and polyamides [22-24]. Concerning their fatigue crack growth properties, a significant amount of published work can

be found for neat polymers such as polyethylene [25], polycarbonate [26], polyethylene terephthalate [27] and polyamide [28, 29]. In particular it has been shown that the molar mass of the polymer has a significant effect on the fatigue properties. The higher the molar mass, the slower the crack propagation rate. However, for fibre reinforced composite materials, very few studies can be found where the molar mass is directly linked with a given mechanical property. An exception is the work of Le Gac and Fayolle [30], who in 2018 studied the tensile behaviour of short glass reinforced polyamide 6.6 composites during aging while following the molar mass. Also, in recent work, the authors investigated the change in the fracture toughness (G_{IC}) induced by aging on carbon/polyamide 6 composites, and it was demonstrated that the fracture toughness after hydrolytic aging can be directly linked with the molar mass of the matrix [31]. It is therefore of particular interest to investigate whether this is also valid under fatigue loading. To the knowledge of the authors, no work has been reported concerning the correlation between the molar mass and the fatigue crack growth properties on long carbon fibre reinforced thermoplastic composites.

The aim of this paper is to investigate the fatigue crack growth properties of C/PA6 composites subjected to wet aging. To do so, the fatigue crack growth properties are first determined experimentally using the multi ΔG control method after different aging conditions. Afterwards, focus is placed on the effect of aging at a given ΔG value. The Time-Temperature Superposition (TTS) principle was then checked before and after aging using the Miyano approach [32]. Then, the fatigue properties were compared to the losses in molar mass observed during hydrolysis. Finally, the experimental data are described using the Hartman-Schijve relationship.

2. Materials & methods

2.1. Materials

The material used in this study is a C/PA6 thermoplastic composite material from Celanese (Reference: CFR-TP-PA6-CF60-01). It was supplied in the form of unidirectional prepreg sheets (125 µm thick) with a fibre volume fraction of 48%. Panel were manufactured by stacking 40 prepreg sheets in a mould. A FEP insert (dimensions 280 x 80 x 0.025 mm^3) was located at mid-thickness at one end of each panel to create a starter crack. The panels were consoidated by heating the mould at 240°C under a pressure of 5 bars. The cooling rate was about 20°C/min. Such a process allowed us to obtain panels with dimensions of 280 x 280 x 5 mm^3. The crystallinity ratio was then measured by DSC and is equal to 38% and the initial molar mass 26.2 kg/mol. Additional properties for the composite are found in Table 1 below.

Property	Value
T_g (°C)	66
Water uptake at saturation after immersion at 25°C (%)	3
E_1 (GPa)	105.6
E_2 (GPa)	5.8
G_{12} (GPa)	2.4
σ_1 (MPa)	1808
σ_2 (MPa)	25
τ_{12} (MPa)	37

Table 1: Composite properties, from [33]

2.2. Aging

Aging was carried out in deionized water at different temperatures ranging from 100°C up to 140°C for durations up to 3 months. To ensure that the water remained liquid during aging, a pressure of 15 bars was applied. The choice of high temperatures for this study (T>100°C) is based on the work of Deshoulles et al. [24]. When polyamide 6 is fully saturated with water in immersion, its glass transition temperature (T_g) decreases from 66°C down to -12°C [34]. Such a loss implies a change in state from the glassy to the rubbery state at ambient temperature. This means that when polyamide 6 is immersed in water at ambient temperature, it will eventually pass into the rubbery state. Therefore, once saturated the polyamide 6 matrix is in the rubbery state both at 25°C and at 140°C. Also, at these temperatures, water diffusion is very fast, so for all aging conditions specimens were fully saturated with water resulting in a homogeneous water profile. As an example, in [31], at 120°C, specimens are saturated after only one day of aging. Additionally, the oxygen contained within the deionized water was removed using nitrogen bubbling (for 3 hours) prior to aging. The choice of removing the oxygen from water is justified by the fact that oxidative aging tends to produce a degradation that mainly occurs on the surface of the specimens. With the 5 mm thick specimens used within this study, a degradation profile through the thickness would therefore be observed. On the other hand, pure hydrolytic aging, i.e. aging in water without oxygen, induces a homogeneous degradation through the thickness and therefore a homogenous molar mass. This is more pertinent when the aim is to link a given property (in this study the fatigue crack growth properties) with the molar mass.

Concerning the latter, molar mass measurements were carried out by the Peak Expert Company using the Laun et al. method [35]. Samples of 10 mg were dissolved with hexafluoroisopropanol (HFiP) for 24h. Calibration was performed using PMMA standards with molar mass ranging from 800 to 1,600,000 g/mol. From these measurements, both the average molar mass in number M_n and average molecular weight M_w were obtained. Here, the value of M_n was used but M_w was also suitable because of the stable polydispersity index during aging.

2.3. Multi ΔG control method

2.3.1. Test specimens

The DCB specimens were produced by water jet cutting to the following dimensions: 250 x 20 x 5 mm^3. The initial crack length a_0 was about 60 mm and instead of aluminium tabs, glass/polyamide 6 tabs were used. This ensures a better interface with the DCB specimens. Tabs dimensions were 20 x 20 x 10 mm^3. For each aging condition three specimens were tested, and all specimens were dried in humidity chambers at 60°C at 0% humidity for about a month prior to testing until stable weight was reached. It was initially intended to test the specimens in the saturated state, however, such tests were not possible. The upper arm from the DCB specimen systematically failed before any crack propagation. This is due to the loss in matrix dominated properties induced by water ingress that also affect flexural strength [33]. In total, 55 specimens were tested (4 in the unaged state and 51 after aging). All specimens were pre-cracked under mode I loading before the fatigue test. The length of the pre-crack was about 10 mm for all specimens. Finally, DCB tests were chosen to investigate the crack delamination in composite as no other simple alternative were found in literature, despite the well know fibre bridging issue. Additionally, in order to investigate the long-term behavior of such composites, using the same test before and after aging allows changes due to aging to be revealed.

2.3.2. Test method

Multi ΔG-control fatigue tests were performed with an MTS Acumen 3 Electrodynamic test system at a frequency of 2 Hz and an R-ratio of 0.1. As stated in the introduction, the G-control method was developed by Manca et al. in [10] and the authors extended this method to a multi ΔG control test method [11]. The latter was implemented within the MTS software (Multipurpose Elite™) to perform the fatigue tests. It should be noted that the multi ΔG control method relies on compliance monitoring throughout the tests. This is essential in order to maintain the cyclic energy release rate ΔG (G_{max}-G_{min}) and R-ratio constant, by adjusting the minimum and maximum displacements continuously as the crack extends.

The compliance C is defined in Eq. 1.

$$C = \frac{\delta}{P} \quad \text{Eq.1}$$

Where δ is the crack opening displacement and P the associated load. Based on this compliance measurement, the crack length a can be calculated, Eq. 2.

$$a = \sqrt[3]{\frac{3EIC}{2}} \quad \text{Eq.2}$$

Where I is the moment of inertia of each DCB arm and E the modulus of the specimen in the longitudinal direction (taken here as 105.6 GPa [33]). The R-ratio is defined in Eq.3 both in terms of displacement and load. It can also be expressed in terms of G_{min} and G_{max}, Eq.4.

$$R = \frac{P_{min}}{P_{max}} = \frac{\delta_{min}}{\delta_{max}} \quad \text{Eq.3}$$

$$R_G = \frac{G_{min}}{G_{max}} = R^2 \quad \text{Eq.4}$$

The cyclic energy release rate ΔG is then expressed as follows, Eq. 5:

$$\Delta G = \frac{9EI}{4ba^4}\delta_{max}^2(1 - R^2) \quad \text{Eq.5}$$

Where b is the width of the DCB specimen. Finally, two requirements must be satisfied to ensure a constant ΔG as the crack grows longer, Eq. 6 and Eq. 7.

$$\frac{\delta_{max}}{a^2} = k \quad \text{Eq.6}$$

$$\delta_{min} = R\delta_{max} \quad \text{Eq.7}$$

Where k is a constant. Once all these equations are defined, the test methodology can be described. First, the operator defines the frequency f, the R-ratio, the number of cycles N to be performed at each ΔG level, the initial ΔG_0 level at which the test will start and finally the $\Delta G_{increment}$ value. The methodology is presented in Figure 1, from [11].

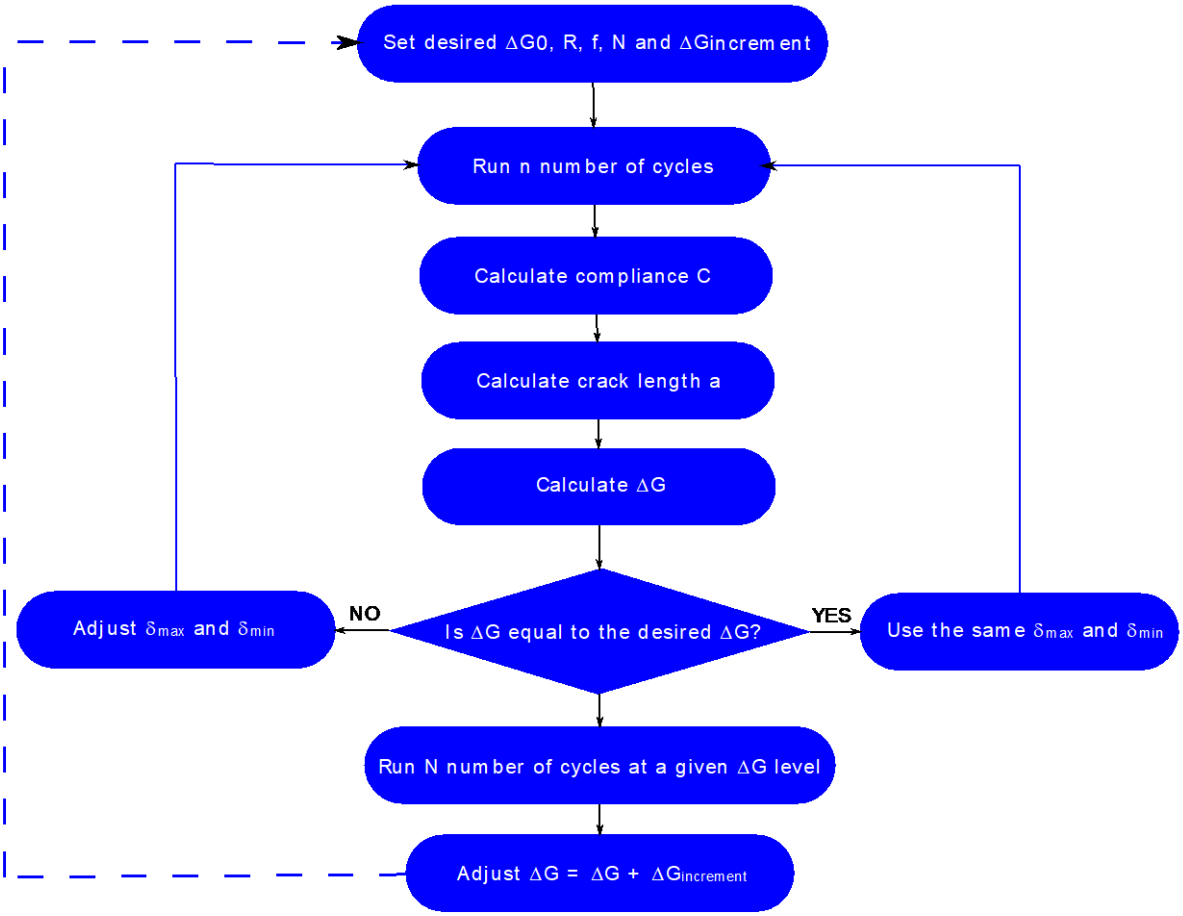

Figure 1: Flowchart of the multi ΔG control method [11]

The test starts at a targeted ΔG_0 value. To keep this value constant, the algorithm first runs n cycles and calculates the compliance. Based on that measurement, the calculation of the crack length is possible and this allows the determination of ΔG, Eq. 5. Once this process is finished, the calculated ΔG value ($\Delta G_{calculated}$) is compared to the targeted value ($\Delta G_{command}$). If the value is within the error defined by the operator ($\Delta G_{tolerance}$), another set of n cycles (here 10 cycles) is performed; if not, the maximum and minimum displacements are adjusted to reach the targeted $\Delta G_{command}$ and so on. When the N number of cycles (here 10 000) at the targeted $\Delta G_{command}$ value are completed, the ΔG value can be increased to $\Delta G_n = \Delta G_{n-1} + \Delta G_{increment}$, the same process as explained above is followed until the measurements no longer respect LEFM (here when d/a>0.4).

2.3.3. Test parameters used in the multi ΔG control tests before and after aging

Figure 1 shows that prior to testing, some parameters need to be entered into the algorithm, i.e. ΔG_0, $\Delta G_{increment}$, $\Delta G_{tolerance}$, N, f and R. For all tests performed here, most of the parameters were the same before and after aging (f, R, N, $\Delta G_{increment}$ and $\Delta G_{tolerance}$). For all tests, $\Delta G_{increment}$ and $\Delta G_{tolerance}$ were taken as 100 and 10 J/m², respectively. However, the initial ΔG_0 value was modified in the case of the aged specimens. Indeed, it was shown in [31] that the G_{IC} value decreased with aging so it is necessary to consider this loss in the fatigue tests. In [11], the initial ΔG_0 was equal to 500 J/m². Compared with the unaged G_{IC} value equal to 3140 J/m², it means that $\frac{\Delta G_0}{G_{IC}} \approx 0.15$. This ratio around 0.15 was then kept for all aging conditions. For the aging conditions at 120°C, the ΔG_0 values are shown in Table 1 along with the G_{IC} values taken from [31] for propagation. The ΔG_0 values at the other aging temperatures (100, 130 and 140°C) can be found in the Appendix.

Table 1: Test parameters for the multi-ΔG tests in the unaged state and after aging at 120°C

Aging time (days)	ΔG_0 (J/m²)	$G_{IC\ prop}$ (kJ/m²) (from [31])
0	500	3410 ± 260
3	500	3302 ± 160
7	400	2490 ± 150
14	300	1560 ± 160
21	200	1210 ± 80
28	100	950 ± 100

2.4. Scanning Electron Microscopy (SEM)

A Philips FEI Quanta 200 SEM was used to examine the fracture surfaces of the tested specimens before and after aging, to investigate whether aging has an effect on the failure mechanism in fatigue.

2.5. Hartman-Schijve representation

Since its first introduction in 1961 [13], the Paris's law, Eq.8, has been extensively used to describe the fatigue crack growth behavior in a wide range of materials.

$$\frac{da}{dN} = C\Delta G^m \qquad \text{Eq.8}$$

where da/dN is the fatigue crack growth rate in m/cycle and C and m are two fitting parameters. Such a representation of the fatigue crack growth suggests a log-linear relationship between da/dN and ΔG (Regime II),

as shown in Figure 2. However, in the literature, it has been shown that in several cases, this law is not sufficient to describe the complete fatigue crack growth behavior, from slow to fast crack propagation rates. Figure 2 shows that the crack growth behaviour can be characterized by three distinct fatigue crack propagation regimes (threshold, log linear and critical [36] corresponding to regimes I, II and III, respectively).

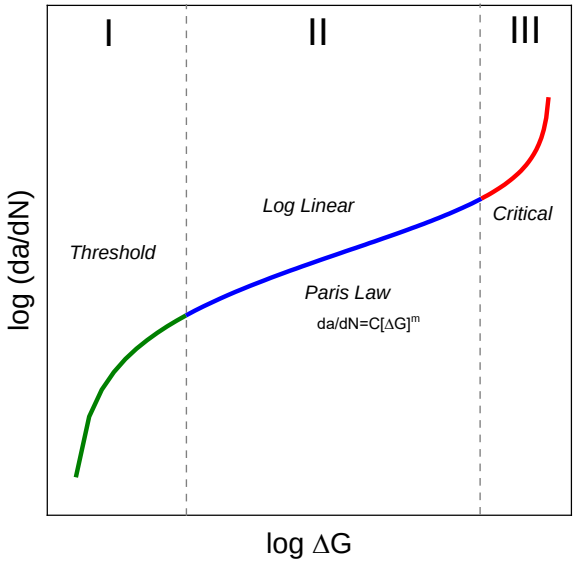

Figure 2: Fatigue crack growth behaviour

Therefore, the Hartman-Schijve relationship was introduced in 1970 for metals [12] and was more recently extended to composite materials [15]. Additionally, the relationship was already used to describe the fatigue crack growth properties of unaged C/PA6 composites in [11]. The Hartman-Schijve equation is presented below, Eq.9.

$$\frac{da}{dN} = D\left[\frac{\Delta\sqrt{G} - \Delta\sqrt{G_{thr}}}{\sqrt{\left[1 - \sqrt{\frac{G_{max}}{A}}\right]}}\right]^n \qquad \text{Eq.9}$$

Where $\Delta\sqrt{G}$ and $\Delta\sqrt{G_{th}}$ are defined in Eq.10 and Eq.11. $\Delta\sqrt{G_{th}}$ is associated with the threshold region and represents the lower bound of the sigmoid (Regime I). D and n are two fitting parameters that respectively represent the slope and exponent of the log linear region (regime II). Finally, A is expressed in J/m² and is associated with the upper bound of the sigmoid (critical region, regime III). It may be noted that some authors have indicated that A can be associated with G_{IC} [14, 15].

$$\Delta\sqrt{G} = \sqrt{G_{max}} - \sqrt{G_{min}} \qquad \text{Eq.10}$$

$$\Delta\sqrt{G_{thr}} = \sqrt{G_{thr\,max}} - \sqrt{G_{thr\,min}} \quad \text{Eq.11}$$

The identification of the different parameters was performed on each specimen tested in this study and a manual fitting was used. First, $\Delta\sqrt{G_{th}}$ and A which respectively represent the lower and upper bounds are directly identified on the experimental data. Based on this, D and m are obtained by plotting da/dN as a function of $(\Delta\sqrt{G} - \Delta\sqrt{G_{thr}})/\sqrt{1-\sqrt{G_{max}/A}}$, as performed in [11, 15].

3. Results & Discussion

This section is first devoted to the results from fatigue crack growth tests performed after aging at different temperatures (100, 120, 130 and 140°C) and for different durations. Second, focus is then placed on the crack growth behavior at an arbitrary ΔG value of 1000 J/m². Then based on Miyano's work [32], the Time-Temperature Superposition (TTS) approach was used to propose a prediction of the long-term behavior, followed by a discussion on embrittlement upon aging. Finally, the Hartman-Schijve representation was used to describe the experimental data.

3.1. Effect of aging on the fatigue crack growth behavior

Figure 3 first shows the results from fatigue tests performed before and after aging using the multi-ΔG control test method. First, the results from fatigue tests in the unaged state (black squares) show that the crack growth behaviour is characterized by three distinct fatigue crack propagation regimes, as described in section 2.5.

Then, let us consider the results from fatigue tests performed after wet aging at 100°C, Figure 3.a. Aging was carried out for durations ranging from 14 up to 90 days. First, results show that scatter is quite low for all conditions investigated. Second, results show that as the aging duration increases, the fatigue crack growth properties are shifted towards faster crack propagation rates. As an example, the crack growth rate at a ΔG value of 1000 J/m² is about 10^{-7} m/cycle in the unaged state while after 90 days of aging at 100°C, it is increased by a decade with a new value of about 10^{-6} m/cycle. This clearly demonstrates the changes induced by aging. A similar trend is observed for all the aging temperatures investigated here, Figure 3.b, 3.c and 3.d, i.e. longer aging durations result in faster crack propagation rates. To further understand this, the following section is focused on the fatigue crack growth behavior at a ΔG value of 1000 J/m².

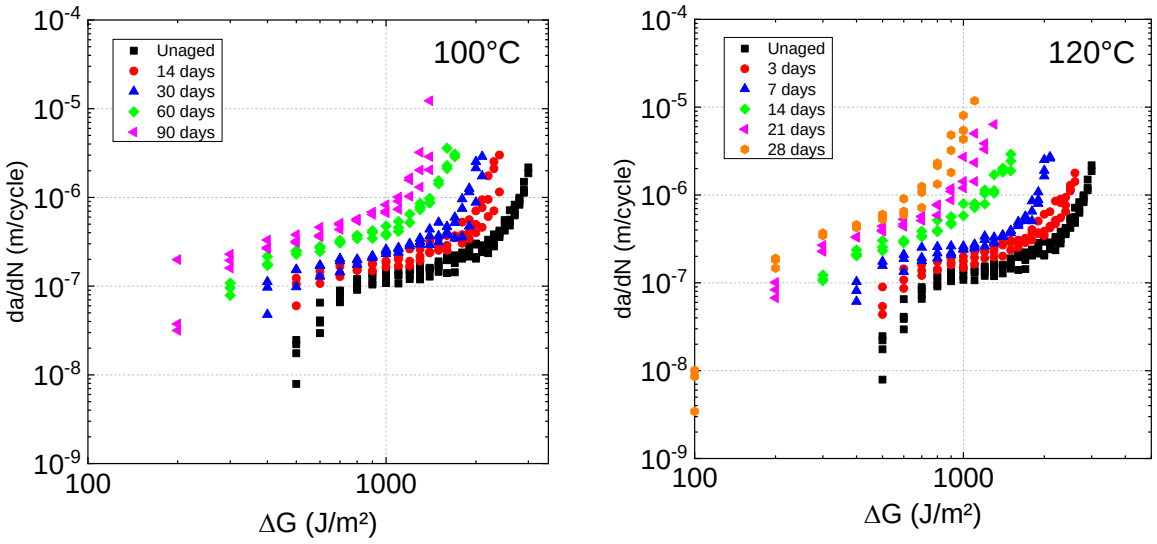

(a) (b)

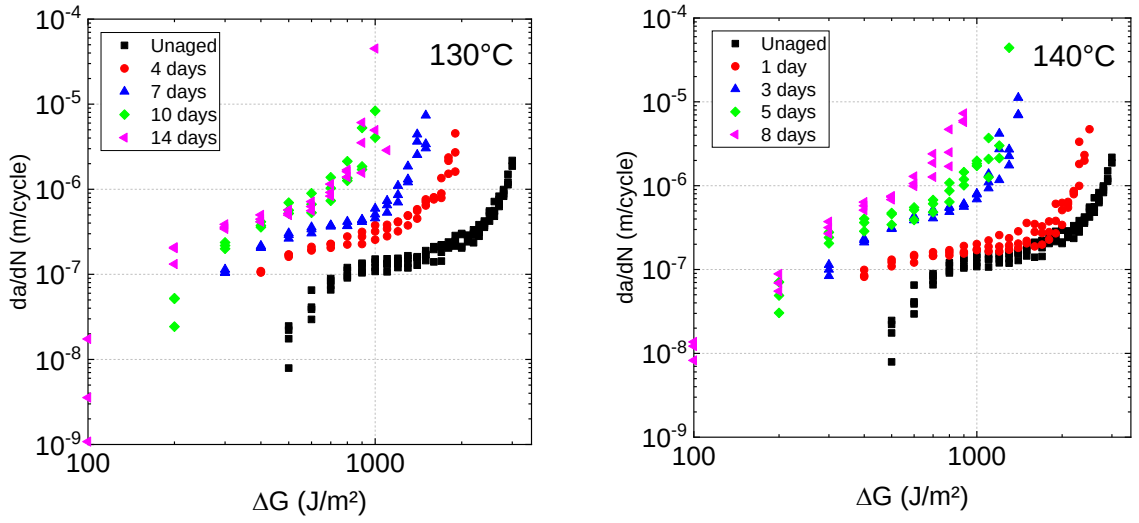

(c) (d)

Figure 3: Fatigue crack growth rate as a function of ΔG after aging at different temperatures and durations (a) 100°C (b) 120°C (c) 130°C (d) 140°C

3.2. Fatigue and fracture behaviour at ΔG=1000 J/m²

3.2.1. Time-Temperature Superposition (TTS)

Based on Figure 3, the crack growth rates at a ΔG value of 1000 J/m² were extracted for all conditions investigated and plotted as a function of time, as shown in the left side of Figure 4. It is observed that as aging duration increases, the fatigue crack propagation rate increases linearly. Then, the right side of Figure 4 shows the

master curve of da/dN for ΔG=1000 J/m². It was obtained using the Miyano approach [32], by shifting da/dN with a coefficient a_t, defined in Eq.12, so that all curves can be superimposed.

$$a_T = exp\left[\frac{E_a}{R}\left(\frac{1}{T_{ref}} - \frac{1}{T}\right)\right] \quad \text{Eq.12}$$

Where E_a is the activation energy in kJ/mol, R the gas constant equal to 8.314 J/mol/K, T the temperature in K and T_{ref} the reference temperature taken as 493 K (120°C). Based on this, it is demonstrated that the time-temperature superposition principle is applicable to da/dN for all the aging temperatures investigated in this work. It may be noted that in [37], Miyano also demonstrated that the TTS principle can be applied to the mode I fatigue crack propagation when performing tests at different frequencies and temperatures.

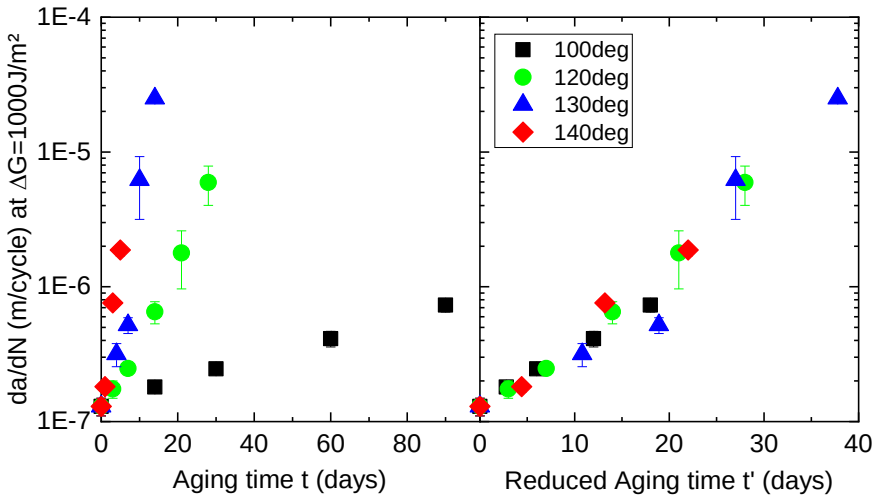

Figure 4: Master curve of the crack growth rate at ΔG=1000 J/m²

The shift factors a_t are now plotted as a function of 1000/RT in Figure 5. The activation energy E_a is then obtained from the slope of $\ln(a_t) = f(\frac{1}{RT})$ and is found equal to 102 kJ/mol with a correlation factor of 0.993.

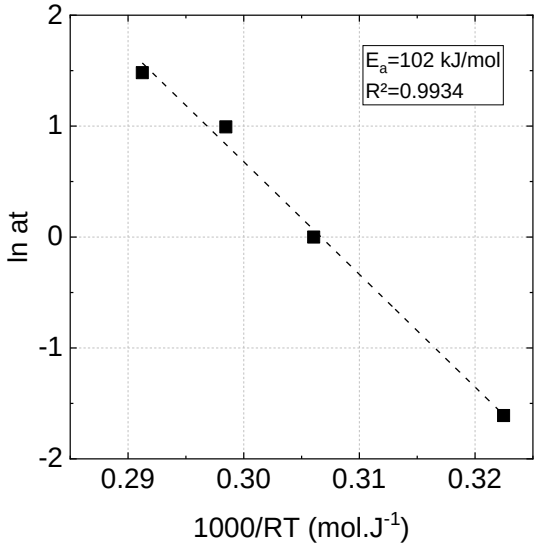

Figure 5: Time-Temperature shift factors and associated activation energy

3.2.2. Effect of molar mass on fatigue crack growth

The molar mass has a significant effect on the mechanical properties of neat polymers. More particularly, as demonstrated by the work of Manson & Hertzberg on several polymers (PMMA, PVC, PA6) [29, 38-40], the work of Kausch [41, 42], and the work of Sauer on polyethylene [43]. These studies showed that the higher the molar mass the lower the crack growth rate.

However, few results are available for composite materials [30, 31]. In [31], the authors recently investigated the effect of hydrolytic aging on the static mode I fracture crack growth properties of C/PA6, using the same specimens as those of this study. In that work, a correlation with the molar mass before and after aging was found. The aging conditions (temperature and durations) were exactly the same as those used in this paper.

Figure 6 shows the change in molar mass as a function of aging time for different aging temperatures, from [31]. Results show that for each aging condition, there is a decrease in the molar mass. The latter is due to the hydrolysis of the amorphous phase of the polyamide 6, which involves a chain scission process when specimens are immersed in water [24]. It is also observed that the higher the temperature, the faster the decrease in molar mass, as expected.

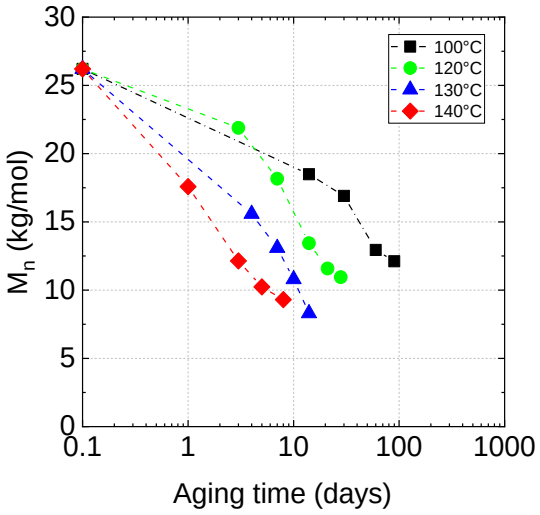

Figure 6: Effect of aging on the molar mass of the PA6 matrix, from [30]

The crack growth rates obtained at ΔG=1000 J/m² are now plotted as a function of molar mass in Figure 7, similarly to that performed by Manson & Hertzberg on PMMA in [38]. Is is observed that da/dN is increased when lowering M_n. Additionally, two different slopes are identified on this da/dN=f(M_n) plot. Indeed, a change in slope is observed at a given M_n value around 15 kg/mol. Below this value, da/dN increases significantly. This suggests a change in mechanical behavior.

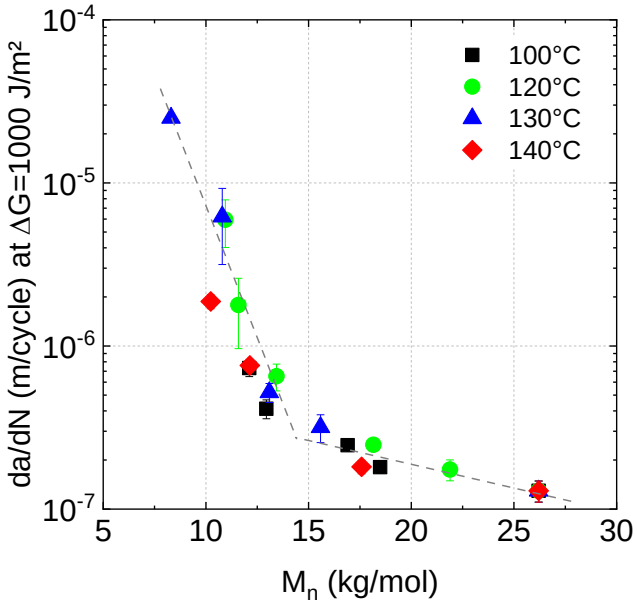

Figure 7: Effect of molar mass in number on the fatigue crack propagation rate at ΔG=1000 J/m²

In the case of amorphous polymers, the loss in fatigue crack growth properties has been explained by the behavior of crazes, which provide a barrier to crack propagation [41]. However, for crystalline polymers, fewer published results are available. Several explanations can be proposed. First, the strength of crystalline polymers depends on their ability to transfer stresses between the amorphous and crystalline phases. In the literature, this has been explained with tie molecules. In particular, it has been shown in [24] for PA6 that a decrease in strain at break during aging was linked with a decrease in tie molecules probability content. Another explanation concerns the loss in entanglements induced by aging; hydrolysis involves chain scission which shortens the length of polymer chains, as witnessed on Figure 6. It is also known from literature that when the length of the polymer chains falls below a critical molar mass M'_c, there are no longer enough entanglements to transfer stresses within the material, which induces in change in mechanical behavior from ductile to brittle [18-21, 24, 31].

To confirm this, the fracture surfaces of specimens tested in the unaged state and after 14 days of aging at 120°C are shown in Figure 8. To obtain these images the tested specimens were cut in three pieces, each corresponding to one of the three identified crack propagation regimes (threshold, log linear and critical).

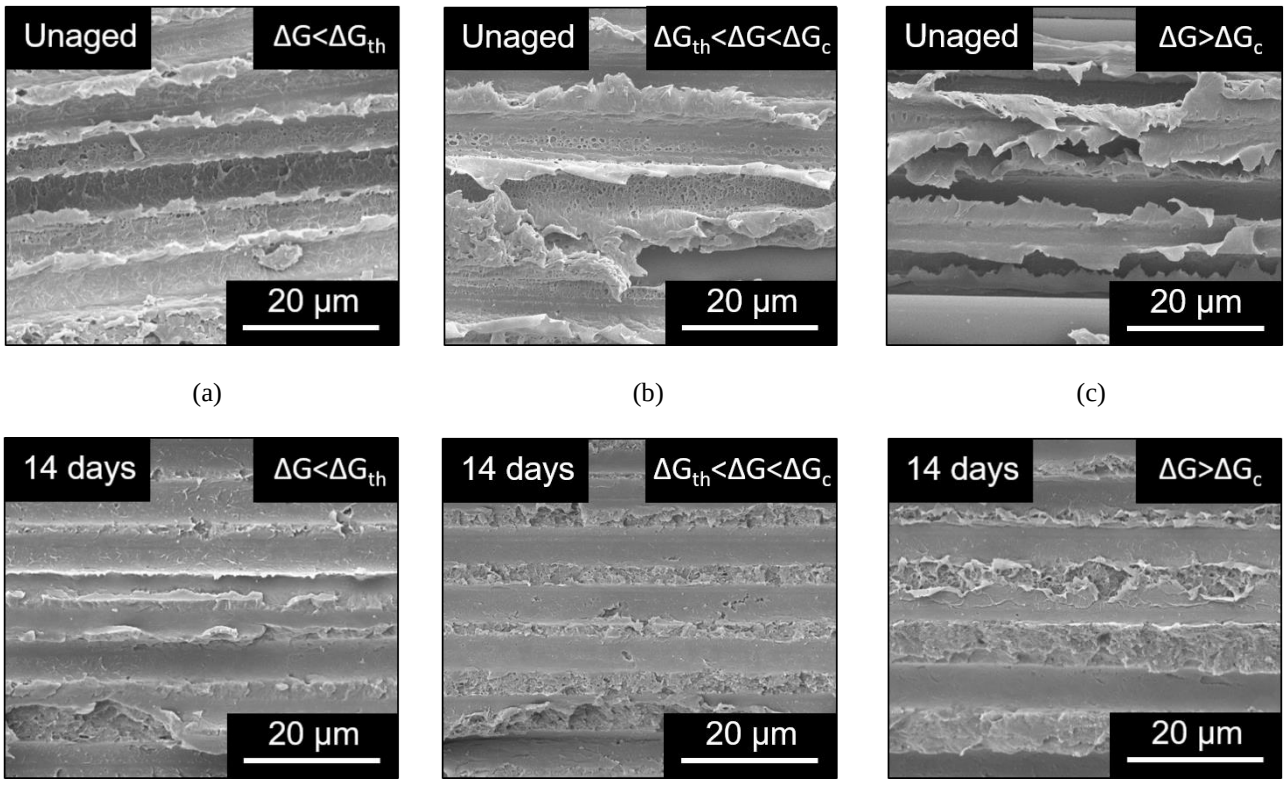

Figure 8: SEM fracture surfaces taken from different crack growth regimes in the unaged state (a) $\Delta G<\Delta G_{th}$ (b) $\Delta G_{th}<\Delta G<\Delta G_c$ (c) $\Delta G>\Delta G_c$ and after 14 days of aging at 120°C (d) $\Delta G<\Delta G_{th}$ (e) $\Delta G_{th}<\Delta G<\Delta G_c$ (f) $\Delta G>\Delta G_c$

Three different aspects can be discussed based on these SEM pictures. First, the fracture surfaces from the specimens tested in the unaged state (Figure 8.a, b and c) show that as the crack propagation increases (from regime I to regime III), the ductility of the matrix appears to increase. Such a result has already been noted in the literature by Karger-Kocsis and colleagues [28] on neat and short fibre reinforced polyamide 6 composites where the ductility of the matrix increased with increasing ΔK and da/dN. Second, on all SEM pictures, it appears that that the strength of the interface is quite poor, even in the unaged state. This was already confirmed in another study on the same material where the transverse tensile strength was found to be 25 MPa [33], i.e. lower than that of a classical C/Epoxy or C/PEEK Material. Additionally, Figure 8.b and Figure 8.c show some fibres that are completely smooth. This indeed suggests a low initial interface. However, despite this low interface strength in the unaged state, high G_{Ic} values were obtained on this material (G_{Ic}=3440 J/m²) [11]. This indicates that it is the high ductility of the PA6 matrix that seems to govern the interlaminar strength rather than the interface, as known from literature on thermosets. Finally, the fracture surfaces of the specimens tested after 14 days of aging at 120°C show very little ductility whatever the crack propagation regime. This indicates that there is a clear change in mechanical behavior upon aging, from ductile to brittle. This was already observed by the authors in [31] when testing carbon fibre reinforced polyamide 6 composites under static mode I loading. As specified earlier, this change from ductile to brittle seems to highlight the fact that after 14 days of aging at 120°C, the molar mass significantly decreases. At this point, the PA6 matrix reaches a level of degradation which does not allow enough entanglements between the polymer chains.

From these SEM images coupled with the results from Figure 7, it appears that the M_n value highlighting the change in slope corresponds this critical molar mass M'_c, identified here as 15 kg/mol. As shown in Table 2, this value is in agreement with results from literature concerning the critical molar mass of PA6.

Table 2: M'_c values for neat PA6 and C/PA6 from this study and published

Source	Material	M'_c (kg/mol)	Assessment of embrittlement	Loading condition
[24]	Neat PA6	15	Yield stress	Static tension
[31]	C/PA6	18	G_{IC}	Mode I Static
This study	C/PA6	15	da/dN	Mode I fatigue

These results have confirmed that there is a strong dependency between the fatigue crack growth properties and the molar mass, as demonstrated in literature on neat polymers. This study has shown that it is also confirmed on long fibre reinforced composite materials.

3.3. Hartman-Schijve representation

Figure 9 now displays the Hartman-Schijve representation for all aging conditions investigated in this work. A good agreement is observed with the experimental data, as shown by the R^2 values given in Table 3. Therefore, it is possible to describe the fatigue crack growth behavior not only in the unaged state but also after aging and extensive degradation, despite a change in mechanical behavior. The values of all four parameters contained within the Hartman-Schijve relationship, i.e. $\Delta\sqrt{G_{th}}$, D, n and A, evolve with aging time. These are found in the Appendix and are represented as a function of aging time.

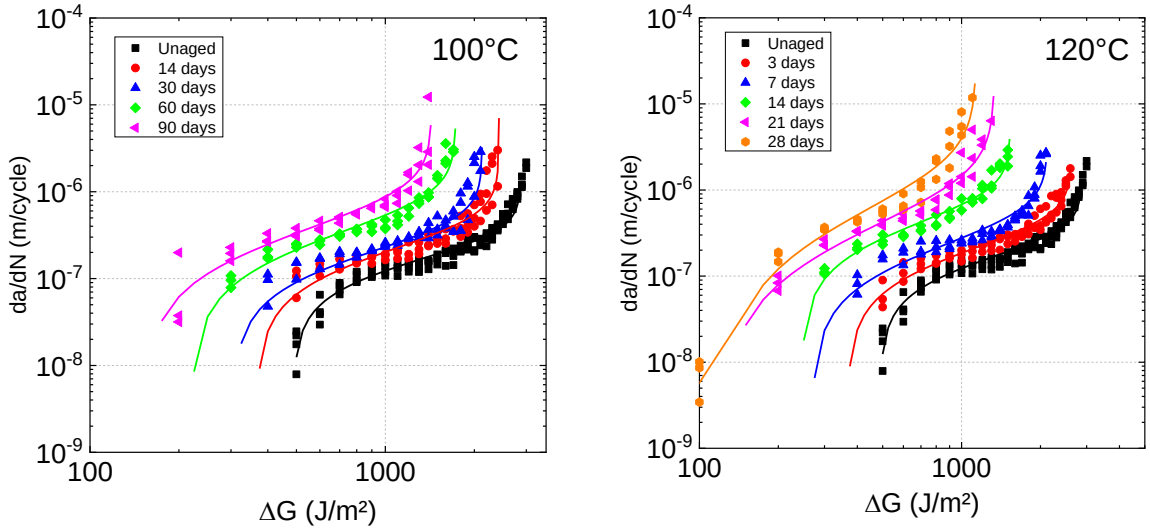

(a) (b)

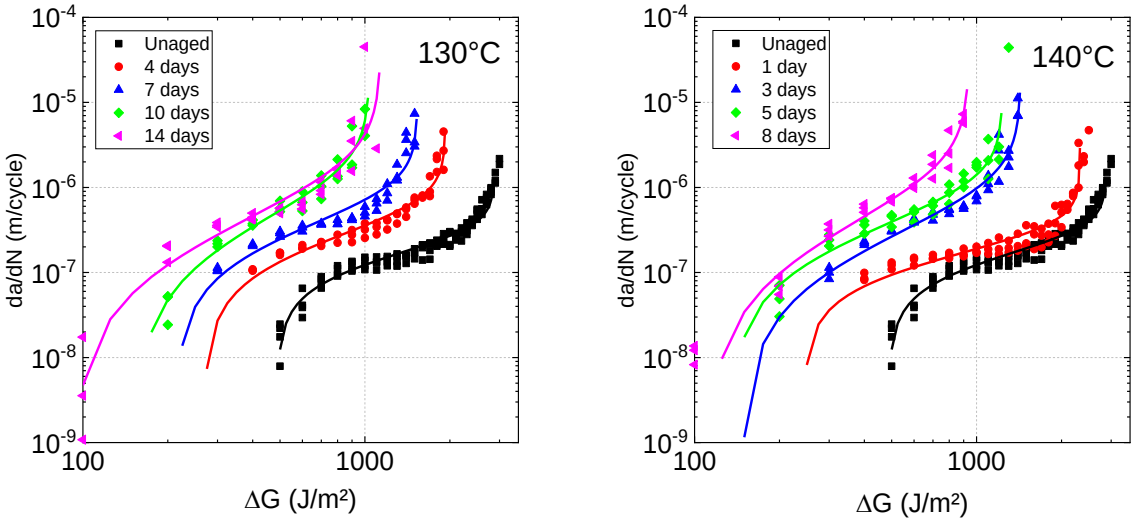

(c) (d)

Figure 9: Fatigue crack growth rate as a function of ΔG and associated Hartman-Schijve representations after aging at different temperatures and durations (a) 100°C (b) 120°C (c) 130°C (d) 140°C

Table 3: Hartman- Schijve representation - R^2 values

Aging temperature (°C)	Aging time (days)	R^2
/	0	0.938
100	14	0.844
	30	0.863
	60	0.935
	90	0.884
120	3	0.928
	7	0.900
	14	0.960
	21	0.936
	28	0.913
130	4	0.928
	7	0.901
	10	0.951
	14	0.882

140	1	0.853
	3	0.944
	5	0.916
	8	0.959

An interesting aspect highlighted in Figure 9 is that in literature, many authors have shown that the static fracture toughness K_{Ic} and strain energy release rate G_{Ic} are fairly insensitive to M_n for values higher that the critical molar mass M'_c. This has been demonstrated on many neat polymers [38-42] and on the same material than that of the current study [31]. This has been explained by the fact that when a polymer chain is long enough, i.e. higher than M'_c, the chain is long enough to span a craze. Therefore, an additional increase in M_n does not have a significant effect.

However, it is observed on Figure 9 that even at the early stages of aging, a shift to higher da/dN is observed despite the fact that Figure 6 shows a drop in molar mass. Therefore, it appears that this material is more sensitive to fatigue crack propagation than in static. This has been observed and partially explained in [38] where they suggests that cyclic loading tends to disentangle the polymer network and that such a phenomena is easier at lower M_n.

The following question can now be raised. Does the parameter A from the Hartman-Schijve equation equal G_{IC}, as stated in literature [14, 15]? Based on the results of the current study and those of Manson & Hertzberg [38], it appears that it is not the case. However, one hypothesis is that most studies investigating the fatigue crack propagation behavior using the Hartman-Shijve representation was focused on C/Epoxy, i.e. with a thermoset matrix made of a different macromolecular network. The network of a thermoset polymer is linked with strong covalent bonds that may not be sensitive to fatigue loadings, contrary to thermoplastics, as demonstrated here. A second hypothesis is that it is not common to observe a sigmoidal behaviour when performing fatigue crack growth tests on composite materials. Usually, a log linear behaviour is observed and A does not have a major effect on the log linear region, as it basically represents the upper bound of the sigmoid. Therefore, future work may include the static and fatigue crack propagation behavior of C/Epoxy using the multi-ΔG control method developed in this work. Nonetheless, a strong result from this study shows that the fatigue crack growth properties are highly dependent on M_n.

5. Conclusion

The fatigue crack growth behavior of C/PA6 composites subjected to hydrolytic aging was investigated in this paper. C/PA6 DCB specimens were tested in mode I fatigue crack growth tests using the multi-ΔG control method before and after aging. Aging was performed under pure hydrolysis conditions (oxygen-free water) at temperatures ranging from 100°C to 140°C. Results showed that whatever the aging condition, aging induced a significant increase in the crack growth rate (by about a decade) compared to those measured for the unaged state. A change in mechanical behavior from ductile to brittle was witnessed during aging, and allowed the identification of a critical molar mass M'_c of 15 kg/mol. A major result from this work also showed that the fatigue crack growth properties were highly dependent on the molar mass M_n, even at the early stages of aging. Such a dependence was not observed in static, meaning that fatigue loadings are more sensitive to aging. Finally, it was also shown that for all aging conditions, the crack growth rate plot exhibited a sigmoidal shape. This was accurately described using the Hartman-Schijve relationship, as the Paris law is unable to capture the entire sigmoidal behaviour. Compared with the Paris law which contains two parameters (pre-exponential factor D and exponent n), the Hartman-Schijve equation introduces two additional parameters (A and $\Delta\sqrt{G}_{th}$, defining the upper and lower bounds of the sigmoid, respectively).

Acknowledgments

The authors would like to thank the scientific direction of Ifremer for the funding of the REPACOMP project.

References

[1] Harris, B. (Ed.). (2003). Fatigue in composites: science and technology of the fatigue response of fibre-reinforced plastics. Woodhead Publishing.

[2] Talreja, R., & Varna, J. (Eds.). (2015). Modeling damage, fatigue and failure of composite materials. Elsevier.

[3] ASTM International. Standard test method for Mode I fatigue delamination growth onset of unidirectional fiber-reinforced polymer matrix composites, ASTM D6115-97 (Reapproved 2011); 2011.

[4] Brunner, A. J., Murphy, N., & Pinter, G. (2009). Development of a standardized procedure for the characterization of interlaminar delamination propagation in advanced composites under fatigue mode I loading conditions. *Engineering Fracture Mechanics*, 76(18), 2678-2689.

[5] Wilk, J. (2018). Compliance based method for testing fatigue delamination propagation in laminates. *Engineering Fracture Mechanics*, 203, 137-151.

[6] Russell, A. J., & Street, K. N. (1988, January). A constant ΔG test for measuring mode I interlaminar fatigue crack growth rates. In Composite Materials: Testing and Design (Eighth Conference). ASTM International.

[7] Tanaka, K., Tanaka, H., Tsuji, T., & Yamagishi, K. (1995). Effect of stress ratio on mode I propagation of interlaminar fatigue cracks in CFRP. *Zairyo*, *44*(502), 960-966.

[8] Hojo, M., Ochiai, S., Aoki, T., & Ito, H. (1995). Mode I fatigue delamination for CF/PEEK laminates using maximum-energy-release-rate constant tests. *Zairyo*, *44*(502), 953-959.

[9] Sato, N., Hojo, M., & Nishikawa, M. (2015). Intralaminar fatigue crack growth properties of conventional and interlayer toughened CFRP laminate under mode I loading. *Composites Part A: Applied Science and Manufacturing*, *68*, 202-211.

[10] Manca, M., Berggreen, C., & Carlsson, L. A. (2015). G-control fatigue testing for cyclic crack propagation in composite structures. *Engineering Fracture Mechanics*, 149, 375-386.

[11] Arhant, M., Lolive, E., Bonnemains, T., & Davies, P. (2021). Fatigue crack growth properties of carbon-polyamide 6 thermoplastic composites using a multi-ΔG control method. *Engineering Fracture Mechanics*, *252*, 107825.

[12] Hartman, A., & Schijve, J. (1970). The effects of environment and load frequency on the crack propagation law for macro fatigue crack growth in aluminium alloys. *Engineering Fracture Mechanics*, 1(4), 615-631.

[13] Paris, P. C. Gomez, AP, Anderson WE, (1961). A rational analytic theory of fatigue. The trend of engineering, 13, 9-14.

[14] Jones, R., Hu, W., & Kinloch, A. J. (2015). A convenient way to represent fatigue crack growth in structural adhesives. *Fatigue & Fracture of Engineering Materials & Structures*, 38(4), 379-391.

[15] Jones, R., Pitt, S., Brunner, A. J., & Hui, D. (2012). Application of the Hartman–Schijve equation to represent Mode I and Mode II fatigue delamination growth in composites. *Composite Structures*, 94(4), 1343-1351.

[16] Davies, P., & Rajapakse, Y. D. (Eds.). (2014). *Durability of composites in a marine environment* (Vol. 208). Dordrecht: Springer.

[17] Weitsman, Y. J. (2011). *Fluid effects in polymers and polymeric composites*. Springer Science & Business Media.

[18] Fayolle, B., Audouin, L., & Verdu, J. (2003). Radiation induced embrittlement of PTFE. *Polymer*, *44*(9), 2773-2780.

[19] Fayolle, B., Colin, X., Audouin, L., & Verdu, J. (2007). Mechanism of degradation induced embrittlement in polyethylene. *Polymer Degradation and Stability*, *92*(2), 231-238.

[20] Fayolle, B., Audouin, L., & Verdu, J. (2000). Oxidation induced embrittlement in polypropylene—a tensile testing study. *Polymer Degradation and Stability*, *70*(3), 333-340.

[21] Arhant, M., Le Gall, M., Le Gac, P. Y., & Davies, P. (2019). Impact of hydrolytic degradation on mechanical properties of PET-Towards an understanding of microplastics formation. *Polymer Degradation and Stability*, *161*, 175-182.

[22] Jacques, B., Werth, M., Merdas, I., Thominette, F., & Verdu, J. (2002). Hydrolytic ageing of polyamide 11. 1. Hydrolysis kinetics in water. *Polymer*, *43*(24), 6439-6447.

[23] Okamba-Diogo, O., Richaud, E., Verdu, J., Fernagut, F., Guilment, J., & Fayolle, B. (2016). Investigation of polyamide 11 embrittlement during oxidative degradation. *Polymer*, *82*, 49-56.

[24] Deshoulles, Q., Le Gall, M., Dreanno, C., Arhant, M., Stoclet, G., Priour, D., & Le Gac, P. Y. (2021). Origin of embrittlement in Polyamide 6 induced by chemical degradations: mechanisms and governing factors. *Polymer Degradation and Stability*, 109657.

[25] Baker, D. A., Bellare, A., & Pruitt, L. (2003). The effects of degree of crosslinking on the fatigue crack initiation and propagation resistance of orthopedic-grade polyethylene. *Journal of Biomedical Materials Research Part A: An Official Journal of The Society for Biomaterials, The Japanese Society for Biomaterials, and The Australian Society for Biomaterials and the Korean Society for Biomaterials*, *66*(1), 146-154.

[26] Pitman, G., & Ward, I. M. (1980). The molecular weight dependence of fatigue crack propagation in polycarbonate. *Journal of Materials Science*, *15*(3), 635-645.

[27] Ramirez, A., Manson, J. A., & Hertzberg, R. W. (1982). Fatigue crack propagation in amorphous poly (ethylene terephthalate). *Polymer Engineering & Science*, *22*(15), 975-981.

[28] Karger-Kocsis, J. (1990). Effects of processing induced microstructure on the fatigue crack propagation of unfilled and short fibre-reinforced PA-6. *Composites*, *21*(3), 243-254.

[29] Bretz, P. E., Hertzberg, R. W., & Manson, J. A. (1982). The effect of molecular weight on fatigue crack propagation in nylon 66 and polyacetal. *Journal of Applied Polymer Science*, *27*(5), 1707-1717.

[30] Le Gac, P. Y., & Fayolle, B. (2018). Impact of fillers (short glass fibers and rubber) on the hydrolysis-induced embrittlement of polyamide 6.6. *Composites Part B: Engineering*, *153*, 256-263.

[31] Arhant, M., Lolive, E., Bonnemains, T., & Davies, P. (2022). A study of pure hydrolysis of carbon fibre reinforced polyamide 6 composites tested under mode I loading. Composites Part A: Applied Science and Manufacturing, 152, 106719.

[32] Miyano, Y., & Nakada, M. (2018). *Durability of fiber-reinforced polymers*. John Wiley & Sons.

[33] Arhant, M., Le Gac, P. Y., Le Gall, M., Burtin, C., Briançon, C., & Davies, P. (2016). Effect of sea water and humidity on the tensile and compressive properties of carbon-polyamide 6 laminates. *Composites Part A: Applied Science and Manufacturing*, *91*, 250-261.

[34] Arhant, M., Le Gac, P. Y., Le Gall, M., Burtin, C., Briançon, C., & Davies, P. (2016). Modelling the non Fickian water absorption in polyamide 6. *Polymer Degradation and Stability*, *133*, 404-412.

[35] Laun, S., Pasch, H., Longiéras, N., & Degoulet, C. (2008). Molar mass analysis of polyamides-11 and-12 by size exclusion chromatography in HFiP. *Polymer*, *49*(21), 4502-4509.

[36] Pascoe, J. A., Alderliesten, R. C., & Benedictus, R. (2013). Methods for the prediction of fatigue delamination growth in composites and adhesive bonds–a critical review. *Engineering Fracture Mechanics*, *112*, 72-96.

[37] Moromizato, T., Nakada, M., & Miyano, Y. (2012). Applicability of Time–Temperature Superposition Principle to the Mode I Interlaminar Fracture Behavior of CFRP Laminates. *Proceedings of the ECCM15 conference.*

[38] Kim, S. L., Skibo, M., Manson, J. A., & Hertzberg, R. W. (1977). Fatigue crack propagation in poly (methyl methacrylate): effect of molecular weight and internal plasticization. *Polymer Engineering & Science*, *17*(3), 194-203.

[39] Kim, S. L., Janiszewski, J., Skibo, M. D., Manson, J. A., & Hertzberg, R. W. (1979). Effect of molecular weight distribution on fatigue crack propagation in poly (methyl methacrylate). *Polymer Engineering & Science*, *19*(2), 145-150.

[40] Skibo, M., Manson, J. A., Hertzberg, R. W., & Collins, E. A. (1977). Effects of molecular weight and plasticizer on fatigue crack propagation in PVC. *Journal of Macromolecular Science, Part B: Physics*, *14*(4), 525-543.

[41] Kausch, H. H. (2012). *Polymer fracture* (Vol. 2). Springer Science & Business Media.

[42] Kausch, H. H., Gensler, R., Grein, C., Plummer, C. J. G., & Scaramuzzino, P. (1999). Crazing in semicrystalline thermoplastics. *Journal of Macromolecular Science—Physics*, 38(5-6), 803-815.

[43] Sauer, J. A., Foden, E., & Morrow, D. R. (1977). Influence of molecular weight on fatigue behavior of polyethylene and polystyrene. *Polymer Engineering & Science*, *17*(4), 246-250.

Appendix

Table A-1: Test parameters for the multi-ΔG tests in the unaged state and after aging at 100, 130 and 140°C

Aging temperature (°C)	Aging time (days)	ΔG_0 (J/m²)	$G_{IC\ prop}$ (J/m²) (from [30])
/	0	500	3410 ± 260
100	14	500	3302 ± 116
	30	400	2872 ± 143
	60	300	1850 ± 180
	90	200	1540 ± 130
130	4	400	2326 ± 144
	7	300	1600 ± 57
	10	200	1106 ± 111
	14	100	830 ± 98
140	1	400	2850 ± 191
	3	300	1647 ± 159
	5	200	1140 ± 14
	8	100	749 ± 18

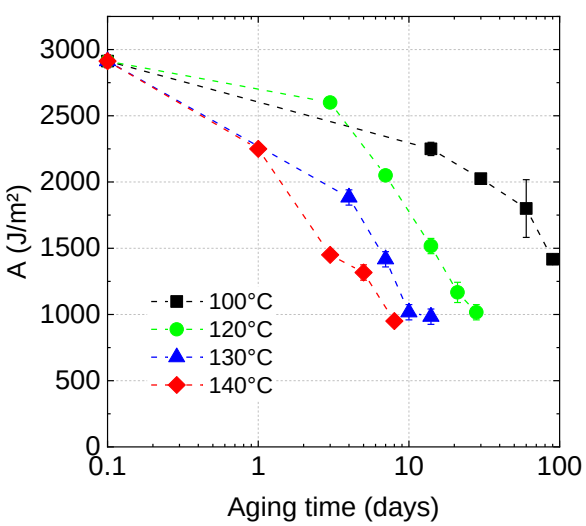

(a)

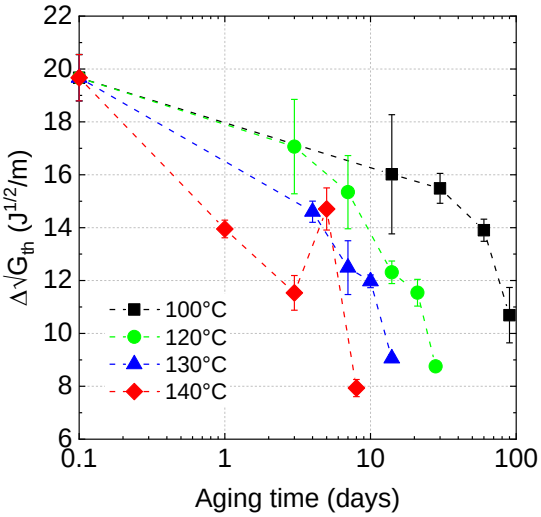

(b)

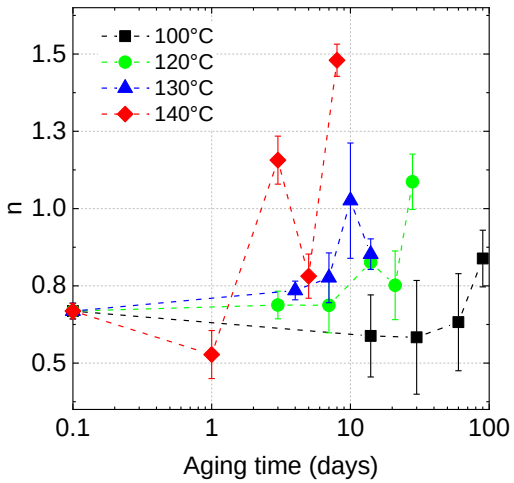

(c)

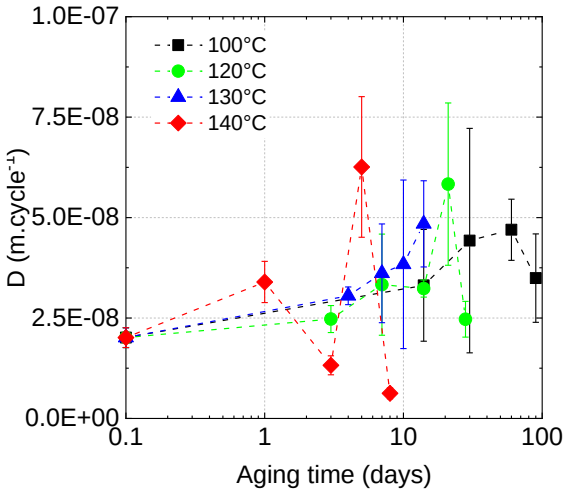

(d)

Figure 4: Parameters from the Hartman-Schijve equation as a function of aging time at 120°C (a) A (b) $\Delta\sqrt{G_{th}}$ (c) n (d) D